Imaging Microglia Surveillance during Sleep-wake Cycles in Freely Behaving Mice

Xiaochun Gu[2,3,6]*, Lifeng Zhang[6], Zhong Zhao[5,6], Huaqiang Fang[6], Ting Zhao[7], Shenghong Ju[2], Xueli Chen[6], Weizheng Gao[4], Xiaoyu Qian[4], Xianhua Wang[1,6], Jue Zhang[4], Heping Cheng[1,6]*

1 National Biomedical Imaging Center, State Key Laboratory of Membrane Biology, Peking-Tsinghua Center for Life Sciences, College of Future Technology, Peking University, Beijing 100871, China

2 Jiangsu Key Laboratory of Molecular and Functional Imaging, Department of Radiology, Zhongda Hospital, Medical School, Southeast University, Nanjing 210009, China

3 Key Laboratory of Developmental Genes and Human Diseases, Department of Histology Embryology, Medical School, Southeast University, Nanjing 210009, China

4 Academy of Advanced Interdisciplinary Study, College of Engineering, Peking University, Beijing 100871, China

5 Institute of Basic Medical Sciences Chinese Academy of Medical Sciences, School of Basic Medicine Peking Union Medical College, Beijing 100005, China.

6 Research Unit of Mitochondria in Brain Diseases, Chinese Academy of Medical Sciences, PKU-Nanjing Institute of Translational Medicine, Nanjing 211899, China

7 Nanjing Raygenitm Biotech Co., Ltd, Nanjing 211899, China

*Address correspondence to: chengp@pku.edu.cn, xiaochun.gu@seu.edu.cn

Abstract

Microglia surveillance manifests itself as dynamic changes in cell morphology and functional remodeling in response to fluctuations in the neural environment. Whether and how microglia surveillance is coupled to brain state switches during natural sleep-wake cycles, as well as under sleep deprivation, remain unclear. To address this question, we used miniature two-photon microscopy (mTPM) to acquire time-lapse high-resolution microglia images of the somatosensory cortex, along with EEG/EMG recordings and behavioral video, in freely-behaving mice. We uncovered fast and robust brain state-dependent changes in microglia surveillance, occurring in parallel with sleep dynamics and early-onset phagocytic microglial contraction during sleep deprivation stress. With the aid of the biosensor $GRAB_{NE2m}$, we also detected local norepinephrine fluctuation occurring in a sleep state-dependent manner. We showed that the locus coeruleus-norepinephrine system, which is crucial to sleep homeostasis, is required for both sleep state-dependent and stress-induced microglial responses and involves β_2-adrenergic receptor signaling. These results provide direct evidence that microglial surveillance is exquisitely tuned to signals and stressors that regulate sleep dynamics and homeostasis so as to adjust its varied roles to complement those of neurons in the brain. *In vivo* imaging with mTPM in freely behaving animals, as demonstrated here, opens a new avenue for future investigation of microglia dynamics and sleep biology in freely behaving animals.

Introduction

Sleep is a highly conserved and essential phenomenon of the brain and serves numerous cognitive as well as metabolic and immunologic functions. Moreover, the sleep-wake transition represents a specific and prominent change in the brain state (Besedovsky et al., 2019; Rasch and Born, 2013). As compared to a wakeful brain, the sleeping brain shows more synchronous neuronal activities, which can be characterized by electroencephalography (EEG). Sleep has two main stages: the non-rapid eye movement (NREM) state, which is thought to promote clearance of metabolic waste partly through increased flow of interstitial fluid (Feng et al., 2019), and the rapid eye movement (REM) state, with EEG patterns similar to wakefulness yet with muscle atonia as well as vivid dreaming in humans (Besedovsky *et al.*, 2019). In addition, sleep, especially NREM, is directly involved in memory consolidation (Fogel and Smith, 2011; Rasch and Born, 2013). However, the underlying biological dynamics and especially the cellular mechanisms of sleep regulation are not entirely understood (Frank, 2019; Frank and Heller, 2019).

As originally suggested by Ramony Cajal (Garcia-Marin et al., 2007), growing evidence shows that microglia dynamics are coupled to and intertwined with the sleep-wake cycle. Microglia are resident innate immune cells ubiquitously distributed in the central nervous system and account for 10–15% of all brain cells (Wolf et al., 2017). Microglia surveillance refers to dynamic changes in cell morphology that accompany functional remodeling in response to changes in the neural environment (Liu et al., 2019; Nimmerjahn et al., 2005; Stowell et al., 2019). It has been shown

that microglia ablation disrupts the maintenance of wakefulness and promotes NREM sleep (Corsi et al., 2021; Liu et al., 2021), while enhancing an animal's fear memory consolidation (Wang et al., 2020). Conversely, acute and chronic sleep deprivation (SD) leads to microglia activation amidst a proinflammatory state triggered by elevated circulating levels of cytokines (C-reactive protein, TNF-α, IL-1, and IL-6) (Krueger et al., 2011). Thus, it is of critical interest to explore whether microglia surveillance can sense and respond to brain state changes during both natural sleep-wake cycles as well as under SD stress.

The investigation of microglial surveillance during the sleep-wake cycle demands technologies suitable to track the rapid dynamics of natural microglia behavior in real time. Though there have been pioneering studies on microglia dynamics in cultured brain slices (Honda et al., 2001), static *ex vivo* conditions can hardly recapitulate the dynamic microenvironments and neuronal activities *in vivo*. Based on results obtained from fixed brain slices, it has been shown that chronic sleep restriction but not acute sleep loss causes microglia process changes (Bellesi et al., 2017), but it is difficult to use this approach to reconstruct the dynamic behavior of microglia accurately and quantitatively. As a major advance, two-photon microcopy has recently been applied to image microglia in head-fixed or anesthetized animals, revealing microglial process motility, chemotaxis and homeostatic translocation, and multifaceted microglia-neuron interactions *in vivo* (Davalos et al., 2005a; Eyo et al., 2018; Liu *et al.*, 2019; Stowell *et al.*, 2019). However, because of mechanical constraints or anesthetics, this technology still precludes experimental paradigms in which natural sleep-wake cycle

is undisturbed. In this regard, the recent advent of miniaturized two-photon microscopy (mTPM) has provided a powerful new tool ideal for fast and high-resolution brain imaging in freely behaving rodents (Zong et al., 2021; Zong et al., 2017). With the aid of mTPM, researchers have mapped the functional network topography of the medial entorhinal cortex (Obenhaus et al., 2022), deciphered the microcircuit dynamics in the dorsomedial prefrontal cortex during social competition (Zhang et al., 2022), and unraveled the specific itch signal processing in the primary somatosensory cortex (Chen et al., 2021).

In this study, we aimed to determine whether microglia surveillance undergoes any significant changes during natural sleep-wake cycles, and if so, what is the underlying regulatory mechanism. Using different models of mTPM tailored for high-resolution, multi-plane or large field-of-view (FOV) imaging, we monitored microglia in the somatosensory cortex of mice during natural sleep-wake cycles or while being subjected to acute SD. We found robust sleep state-dependent and SD-induced changes in microglia surveillance with characteristics differing from those induced by anesthetics. Furthermore, we showed that norepinephrine signals from the axonal projections of the locus coeruleus (LC) and, more specifically, β_2-adrenergic receptor (β_2AR) signaling underlie the state-dependence of microglia surveillance.

Results

Imaging microglia dynamics in freely behaving mice.

To visualize microglial morphology and dynamics during the sleep-wake cycle, microglia were specifically labeled with green fluorescent protein (GFP) expressed under the control of an endogenous Cx3cr1 promoter (Cx3cr1-GFP). Time-lapse imaging of the somatosensory cortex utilized the fast and high-resolution miniature two-photon microscope (FHIRM-TPM) recently developed by our laboratory (Zong *et al.*, 2017), and EEG/Electromyography (EMG) signals and behavior videos were simultaneously recorded to determine corresponding sleep-wake states (Fig. 1a-c and Supplementary Fig. 1). The focal plane of the FHIRM-TPM was placed 50-100 μm beneath the surface of the somatosensory cortex with a field-of-view (FOV) of 220 × 220 μm (Fig. 1d). Under the experimental conditions, we were able to track morphological and positional changes of a cohort of 5-10 microglia at a frame rate of 5 frames per second (FPS) over prolonged durations of greater than 10 hours (Supplementary Fig. 1), while the animals were allowed to roam and behave freely and their sleep-wake cycles remained undisturbed. Though we were initially concerned with potential photoxicity associated with prolonged mTPM imaging, no changes in microglial morphology and fluorescent intensity were evident even after non-stop recording over the entire protocol period (Supplementary Fig. 1). This remarkable result indicates that photo damage is minimal, if any, during *in vivo* imaging (Supplementary Fig. 1).

Dynamic changes in microglial area, branching points, and process end-point speed were then analyzed using Imaris software (Fig. 1 e1-e3′ and Supplementary Fig. 1). We found that individual microglia maintained a relatively stable territory of surveillance over the entire experimental period, even while their individual projections extended and contracted incessantly, giving rise to a process end point motility of 1.39 ± 0.09 μm/min in the wake state (Fig. 1f-h). These results show that mTPM in conjunction with multi-modal recordings of EEG/EMG and behavioral videos enables *in vivo* visualization of microglia dynamics over multiple time scales in freely behaving mice. Interestingly, we also observed occasional short-range translocation in a few cells, suggesting the ability of microglia to survey territories beyond their own boundaries, in general agreement with recent observations in head-fixed mice (Eyo *et al.*, 2018).

Microglia surveillance during the sleep-wake cycle

By simultaneously imaging microglia and recording EEG/EMG throughout a sleep-wake cycle, we obtained continuous 4-6 h datasets from different mice and, in conjunction with video interpretation, segmented and sorted them into subgroups corresponding to wake, NREM, and REM states (Fig. 2a). For each state we quantified morphological features and process motility from 15 cells. Wake and NREM states lasting longer than 15 min were identified, for which the last 5-minute recording was selected, and REM states lasting longer than 5-min for the

characterization of possible state-dependent microglia dynamic surveillance.

We found that during the NREM and REM states, microglial process length and surveillance area increased compared with those during wakefulness (Fig. 2b-d, b′-d′). Concomitantly, the number of branching points significantly increased, while end-point moving speed of microglial processes decreased (Fig. 2e-h), indicating state-dependent changes in microglial morphology as well as process motility under natural sleep-wake cycles. To provide a volumetric view of the dynamics of microglial morphology, we adapted our latest version of mTPM with an electrical tunable lens (ETL) capable of imaging variable focal planes (Zong *et al.*, 2021) (Fig. 2i-o and Supplementary Fig. 2). Multi-plane reconstruction revealed more extended process lengths and greater branch point numbers as compared to single-plane imaging as expected (Fig. 2l, n). The volume of surveillance for individual microglia changed from 1661 ± 264.4 μm^3 in the wake state to 3802 ± 670.5 μm^3 in REM state and 4616 ± 324.6 μm^3 in NREM state (Fig. 2m). Similar to results obtained with single-plane imaging, the end-point speed of processes decreased in REM and NREM compared to the wake state (Fig. 2o). While both REM and NREM had the same trends in change as compared to the wake state, significantly greater changes were associated with NREM than REM in terms of cell volume, branch length, branch number, and end-point speed (Fig. 2l-o). These results demonstrate differential microglial dynamic surveillance as the brain state switches among wakefulness, REM and NREM, and the state-dependent morphological and process-motility changes can be robustly reproduced with either single-plane or volumetric imaging. Intriguingly, microglia can

even sense and respond to subtle differences between REM and NREM states. Because more extended microglia are thought to have greater surveillance ability (Kierdorf and Prinz, 2017), our results support the notion that microglia during the NREM and REM periods tend to be more active in the opportune clearing of metabolic wastes accumulated during the wake states.

To this end, it is also instructive to compare and contrast REM/NREM state-dependent characteristics with those induced by anesthesia. In mice under isoflurane (1.2% in air) for 20-30 min, we found that microglial length, area, number of branching points (Supplementary Fig. 2) were similarly increased compared with the wake state, as was the case in NREM and REM. However, the end-point movement of processes exhibited opposite changes (Liu *et al.*, 2019), increasing with anesthesia but decreasing in sleep states (Fig. 2h, o and Supplementary Fig. 2). This result shows that microglia surveillance appears to differ qualitatively between sleep and anesthesia states.

Acute SD promotes contraction of microglial processes.

Sleep loss is detrimental to brain function and results in structural plastic changes in nerve cells. Whether microglia dynamic surveillance alters after sleep loss remains controversial (Bellesi *et al.*, 2017; Wang *et al.*, 2020). Therefore, we induced acute SD in mice by forcing the animals to exercise and interrupting sleep with a rotatory rod, starting at 9:00 am and lasting for six hours (Fig. 3a). In the wake state,

microglia typically exhibited an extended form with ramified, long, thin processes. Overt morphological changes occurred as early as 3h after SD, when microglia presented a contracted form bearing short and thick processes. By 6h, nearly all microglia cells were converted into a phagocytic form, assuming an amoeboid shape with few processes (Fig. 3b-d). We found that microglial length, area and number of branching points decreased with the continuous SD (Fig. 3e-h). Changes in the end-point speed of processes appeared to be biphasic, increasing at 3h SD and then declining below baseline level at 6h SD (Fig. 3h); the latter may result in part from the dramatic shrinkage of the processes. Thus, our real-time recording in live animals clearly demonstrates that SD stress induces microglia to assume an active state and conspicuous microglial response occurs early in SD.

NE changes in somatosensory cortex during the sleep-wake cycle

Next, we sought to determine a possible signaling mechanism(s) that incites microglia surveillance state- and stress-dependent changes. Among a number of candidates responsible for stress responses, norepinephrine (NE) has recently been shown to play a crucial role in microglia surveillance by responding to neuronal network activity (Liu *et al.*, 2019) and partaking of synaptic plasticity (Stowell *et al.*, 2019). Therefore, we combined mTPM imaging with EEG and EMG recording to determine whether NE levels in the somatosensory cortex fluctuate during the sleep-wake cycle to control microglia surveillance. We imaged extracellular NE dynamics

in somatosensory cortical neurons with NE biosensor $GRAB_{NE2m}$ (Fig. 4a), which was developed based on G protein receptors (Feng *et al.*, 2019; Kjaerby et al., 2022). The biosensor was expressed on the plasma membrane of neurons to report the dynamic change of the extracellular NE. Dynamic changes of NE levels was evident in the somatosensory cortex during wake, NREM and REM states (Fig. 4b). NE levels reached higher levels during longer awakenings, while the lowest NE levels were detected during REM sleep (Fig. 4b) and he largest changes in NE levels were recorded occurred during the transition from REM to wake (Fig. 4b). During NREM sleep, the NE oscillated dynamically around a relatively low level (Fig. 4b), with brief increases that might be related to memory consolidation (Kjaerby *et al.*, 2022). On average, mean levels of NE exhibited a brain-state dependent change, varying in a decreasing order from wake to NREM and to REM (Fig. 4c). These results are in general agreement with recent observations that NE fluctuates in a sleep-state dependent manner in the medial prefrontal cortex, and suggest that NE may play a crucial role in controlling the stage dependent microglial changes.

Role of the LC-NE signal in controlling the microglia dynamic surveillance

To determine possible involvement of NE in sleep state- and SD-induced microglia surveillance, we used the locus coeruleus (LC)-selective neurotoxin, N-(2-chloroethyl)-n-ethyl-2-bromobenzylamine (DSP4; applied 2 days before imaging) to ablate LC axons projecting into the cortex (Gonzalez et al., 1998) (Supplementary Fig.

3) and characterized microglial surveillance with and without an LC-NE signal (Fig. 5a). DSP4 application led to a significant increase in sleep states, particularly NREM sleep (Supplementary Fig. 3), in agreement with previous studies (Gonzalez *et al.*, 1998). In the LC axon-ablated wake state, microglial processes became more contracted as compared to those in control animals (Fig. 5b). Importantly, the sleep state-dependent changes in microglia surveillance were abolished altogether; neither microglial morphology nor process motility displayed any of the previously significant changes seen when the brain states cycled across wake-REM-NREM (Fig. 5b-g). Likewise, DSP4 treatment completely prevented SD-induced alteration of microglia surveillance (Supplementary Fig. 3). These results indicate an essential role for the LC-NE signal in sleep- and stress-dependent state modulation of microglia surveillance.

The effects of the neural modulator NE are mediated by two families of G-protein-coupled receptors, α and β-adrenergic receptors (ARs), each comprising several subtypes. In particular, β_2AR is expressed at high levels in microglia relative to other CNS cell types (Gyoneva and Traynelis, 2013; Mori et al., 2002; Zhang et al., 2014). We, therefore, examined microglia surveillance in β_2AR KO animals during natural sleep-wake cycles and under SD stress. Similar to LC axon ablation, β_2AR KO disturbed wake-sleep homeostasis, as manifested by a lengthening of overall sleep duration (Supplementary Fig. 3). By contrast, removal of β_2ARs failed to abolish dynamic changes in microglia when the brain state switched between sleep and wakefulness (Figure 4H-N). Nonetheless, the ability of microglia to subtly distinguish

between REM and NREM states was largely compromised (Fig. 4h-n and Supplementary Fig. 3), suggesting a partial contribution of β_2AR signaling to LC-NE modulation of microglia surveillance during sleep-wake cycles. Regarding microglia responses to SD stress, we showed that microglial morphology and motility remained unchanged during the SD protocol in β_2AR KO animals (Supplementary Fig. 3), revealing a predominant role for β_2AR signaling in LC-NE modulation of microglia surveillance under SD stress.

Discussion

With the development of mTPM imaging and EEG/EMG recording in freely behaving mice, we now provide direct evidence that microglia surveillance in mouse somatosensory cortex is sleep-state dependent during natural sleep-wake cycles and that microglia contract from ramified into phagocytic forms a few hours after the onset of acute SD stress. Combined with pharmacological intervention and the use of NE biosensor and genetically manipulated animals, we showed that the LC-NE pathway mediates these state-dependent changes in microglia surveillance and that β_2AR signaling is involved in various aspects of the microglial responses, extending recent reports that the same pathway underlies microglia surveillance in the context of neuronal network activity (Liu *et al.*, 2019) and synaptic plasticity (Stowell *et al.*, 2019).

That microglia surveillance is sleep state-dependent substantiates an intimate relationship between rapid, robust state-dependent microglia remodeling and the biology of the sleep-wake cycle (Feng *et al.*, 2019; Frank and Heller, 2019; Xie et al., 2013). It has been shown that microglia play a central role in the removal of metabolic waste and even cell debris from the brain (Huisman et al., 2022; Marquez-Ropero et al., 2020). Our study shows that microglia in the sleeping brain have larger area and length, consistent with greater clearance ability in the sleeping state than the waking. Furthermore, our results show that microglia surveillance significantly differs between REM and NREM sleep in the somatosensory cortex, likely reflecting metabolic and functional differences between the two states. More specifically,

previous reports have proposed differential roles between the NREM and REM sleep for consolidation of different types of memories. For example, NREM sleep contributes to declarative memories, whereas REM sleep is important for procedural and emotional memories (Besedovsky *et al.*, 2019; Rasch and Born, 2013). Memory consolidation is closely related to synaptic plasticity, in which microglia play a very important role (Corsi *et al.*, 2021; Tuan and Lee, 2019). In this regard, our findings hint at the possibility that not all features of microglia-neuron interactions, including mode of action and localization, are equal in the consolidation of different types of memory.

It has been shown that a large proportion of Iba1-immunoreactive microglia with larger cell bodies and less ramified processes appear in hippocampal brain slices following 48-72h of sleep deprivation and in the frontal cortex after 4.5 days of chronic sleep restriction, whereas acute sleep deprivation for 8 hours had no effect on microglial morphology (Bellesi *et al.*, 2017; Hall et al., 2020). However, these findings have mostly been derived from slice staining. While the present work support the general conclusion that microglia surveillance is responsive to SD stress, our real-time mTPM imaging *in vivo* also unmasked a progressive change in microglia surveillance that occurred as early as 3h after onset of SD and full conversion of microglia into the phagocytic form after 6h SD stress. This apparent disparity between the current and previous reports might reflect the complications arising from *ex vivo* sample preparation, because microglia surveillance is highly dynamic and sensitive to neural environmental changes, evidenced by its cyclic changes during the sleep-wake

switch.

We have provided two lines of evidence that the LC-NE-β_2AR axis is involved in microglial surveillance both during natural sleep-wake cycle and under SD stress. Ablation of LC-NE neuronal projection abolished and knockout of β_2ARs markedly altered the manifestation of the state-dependence of microglia surveillance. These findings are well supported by emerging evidence that NE is necessary for microglial activation (Bellesi et al., 2016; Berridge et al., 2012). First, NE is known to be a key neurotransmitter that regulates sleep dynamics (Wang *et al.*, 2020) and the dynamics of microglia (Liu *et al.*, 2019; Sugama et al., 2019), which bears the most β_2ARs among all CNS cell types. Second, β_2AR signaling plays an important role in morphology and chemotaxis (Gyoneva and Traynelis, 2013). Third, microglia-specific knockout of β_2AR abolished the microglial response to neuronal network activity (Liu *et al.*, 2019). Our results also extend the classic view of NE regulation of sleep and wakefulness by revealing a prominent microglial component in the NE response. Because β_2AR knockout failed to abolish microglial responses to sleep state switch and SD stress altogether, further studies are warranted to understand more fully the mechanisms whereby LC-NE signaling regulates microglia surveillance in health and disease.

In summary, by real-time *in vivo* mTPM imaging of microglia surveillance, we uncovered the state-dependence of microglia surveillance during natural sleep-wake cycles and a robust, early-onset response to SD stress. Both types of microglial dynamics are under the regulation of LC-NE with the involvement of β_2ARs as one of

its main effectors. These results highlight that microglia undergo rapid and robust remodeling of both morphology and function to fulfill multimodal roles complementary to those of neurons in the brain. In addition, the methodologies established in the present study may prove to be of broad application for future investigations of microglia dynamics and sleep biology in freely behaving animals.

Acknowledgements

We thank Dr. Wei Xie from Southeast University and Dr. Hailan Hu from Zhejiang University for their carefully reading and valuable comments; L. Wang and T. Zhu from Raygenitm Biotech Co., Ltd, and Y. Guo from the company Transcend Vivoscope for comments on the optics, biological experiments, and data processing; and the Nanjing Brain Observatory for data processing services. The work was supported by grants from the National Science and Technology Innovation 2030 Major Program 2021ZD0202200 and the National Natural Science Foundation of China (81925022, 61975002, 31830036, 31821091, 8182780030 and 61821002), and CAMS Innovation Fund for Medical Sciences (2019-I2M-5-054).

Author contributions

X.G. and H.C. conceived the project and supervised the research; X.G. designed and supervised the biological experiments. X.G. and X.C. performed the experiments and led data analysis and figure-making; X.Q. and W.G. contributed data analysis under

the supervision of H.C., J.Z., and X.G; X.G., L.Z., H.F., and H.C. wrote the manuscript, while all authors participated in discussions and data interpretation.

Competing interests

The authors declare no competing interests.

Methods

Animals

All experimental protocols were carried out with the approval of the Institutional Animal Care and Use Committee of PKU-Nanjing Institute of Translational Medicine (Approval ID: IACUC-2021-023). Male mice, 2-3 months of age, were used in accordance with institutional guidelines. Cx3cr1-GFP (Jax, #021160) heterozygous mice were used to visualize microglia with miniature two-photon microscopy (mTPM). To ablate LC-NE neurons, DSP4 (Sigma, #C8417) solution was administered intraperitoneally (50 mg/kg) twice at 24-h intervals and a minimum of 48 h before mTPM imaging. Adrb2 KO (Jax, #031496) mice were crossed with Cx3cr1-GFP mice to generate (Cx3cr1-GFP+/-; Adrb2-/-) mice, which were used in experiments with β_2-adrenergic receptor knock-out. Mice were housed with a standard 12h light/12h dark cycle and fed standard chow *ad libitum*.

Surgery and electrode implantation

All surgical procedures were done sterilely, and all animal-administered reagents were sterile. Mice were anesthetized with isoflurane (1.5% in air at a flow rate of 0.4 L/min) and maintained on a 37°C heating pad during surgery. The cerebral cortical region to be imaged was localized based on the stereotactic coordinates (somatosensory area, from bregma: anteroposterior, -1 mm, mediolateral, +2 mm) and marked with a fine black dot. The skull over the region of interest was thinned with a high-speed micro-drill under a dissection microscope. Drilling and application of normal saline were done intermittently to avoid overheating and hurting the underlying cerebral tissue. After removing the external layer of the compact bone and most of the spongy bone layer with the drill, the area continued to thinned until an expanded smooth area (~3 mm in diameter) was achieved, making sure the middle was thin enough to get high quality imaging. A drop of saline was applied and a 3-mm-diameter glass coverslip previously sterilized in 70% ethanol was placed on this window, then dental cement was applied around the glass coverslip.

500 nL of AAV9-hSyn-$GRAB_{NE2m}$ (BrainVTA, #PT-2393) were injected into the somatosensory cortex (A/P, -1 mm; M/L, +2 mm; D/V, -0.3mm) at a rate of 50 nL/min. 3-mm-diameter glass coverslip were implanted and fixed on the somatosensory cortex. The mice were used in the experiment one month after postoperative recovery.

Epidural screw electrodes (diameter 0.8 mm) were implanted bilaterally on the opposite sides of the imaging window for constant EEG recording from the frontal

(bregma: anteroposterior, +1.5 mm, mediolateral, +1.5 mm) and parietal cortex (anteroposterior, -2 mm; mediolateral, +2.5 mm). Electrodes were fixed to the skull with dental cement. Another pair of electrodes was inserted into the neck muscles for EMG recording. Then, a headpiece baseplate was attached to the skull with cyanoacrylate and reinforced with dental cement.

Simultaneous imaging and recording

After recovery from surgery, mice with a clear cranial window and typical EEG/EMG signals were selected for further experiments. With the mice head-fixed on the imaging stage, an mTPM imaging stack was first acquired using an mTPM (Transcend Vivoscope), and a proper field-of-view (FOV) with 5-10 microglial somata was located 50-100 μm beneath the pial surface. The holder of the mTPM was then sealed onto the baseplate over the coverslip on the head, and the mTPM could be repetitively mounted and dismounted to track the same population of microglia over different days (Supplementary Fig. 1).

Three models of mTPM were used for different experiments: FHIRM-TPM high-resolution model (Zong *et al.*, 2017) with lens NA of 0.7 and FOV of 220 × 220 μm for Figs. 1-4; headpiece weight was 2.13 g, and lateral and axial resolutions were 0.74 and 6.53 μm, respectively. FHIRM-TPM large FOV model (Zong *et al.*, 2021) with a headpiece weight of 2.45 g, lens NA of 0.5, and FOV of 420 × 420 μm for Supplementary Fig. 3, and lateral and axial resolutions were 1.13 and 12.2 μm, respectively; FHIRM-TPM 2.0 ETL model[2] in Supplementary Fig. 2, with headpiece

weight of 4.3 g, Z-depth range of 45 μm, lens NA of 0.7, lateral resolution of 0.74 μm, axial resolution of 6.53 μm, and FOV of 220 x 220 μm. Images were acquired to visualize the microglial surveillance: time-lapse xy imaging stack at a frame rate of 5 FPS or multi-plane imaging stacks (20 planes at 2 μm intervals, 5 frames/s). Each model of mTPM was equipped with a water-immersion miniature objective and a 920 nm femtosecond fiber laser. Excitation for fluorescence imaging was achieved with 150-fs laser pulses (80 MHz) at 920 nm for GFP with a power of ~25 mW after the objective.

The EEG/EMG signals were recorded continuously and simultaneously by Vital Record (Kissei Comtec system), and mouse behavior was monitored with an infrared video camera. Mice were never disturbed when they were undergoing spontaneous sleep-wake cycles, feeding, or drinking.

Sleep deprivation

Sleep deprivation (SD) was achieved by forcing the mice to move continuously through power devices (Soft maze, #XR-XS108)(Pandi-Perumal et al., 2007). The experimental device consisted of a computer console, a horizontal rotating rod with a diameter of 46 cm and a round mouse cage of 50 cm. The rotating rod can rotate horizontally randomly (3 times/min) in clockwise and counterclockwise directions under the control of the computer. The mouse was placed in the cage one hour per day for one week for habituation. After baseline sleep recording, mice were sleep-

deprived for the duration indicated in each experiment, starting at 9:00 AM and lasting up to 6h into SD.

Anesthesia experiment

Time-lapsed image stacks acquired between 20 and 30 min after anesthesia (isoflurane, 1.5% in air at a flow rate of 0.4 L/min) were used to evaluate microglial dynamic surveillance under anesthetized conditions.

Quantification and statistical analysis

EEG/EMG data analysis

EEG and EMG signals were amplified and filtered as follows: EEG, high-pass filter at 0.1 Hz, low-pass filter at 35 Hz; and EMG, high-pass filter at 10 Hz, low-pass filter at 100 Hz. All signals were digitalized at 128 Hz and stored on a computer. As described previously (Bellesi et al., 2013), EEG power spectra were computed by a fast Fourier transform routine for 10 s epochs. Wake, nonrapid eye movement (NREM) sleep, and REM sleep were manually scored off-line (SleepSign, Kissei Comtec) in 10 s epochs according to standard criteria[4]. Epochs containing artifacts, predominantly during animal movement, were excluded from spectral analysis.

Microglial Morphological Analysis

In order to accurately quantify microglial morphometric changes in different brain states, wake and NREM states lasting longer than 15 min were chosen, among which

the last 5 minutes of recording or a total of 1500 frames was selected, in conjunction with video interpretation, for further processing and analysis. Because they were of relatively short duration, REM states lasting longer than 5 min were used for analysis.

Image stacks were first processed offline using ImageJ software to correct for xy motion artifacts, and the time-lapse stack was aligned using the StackReg plugin. In some experiments, motion artifacts due to Z-level drift was further minimized by collecting multi-plane images over ±20 μm depth at 2 μm intervals and then compressing them into a single xy projection. In this case, corresponding projections were generated over a 5-min window to substitute for time-lapsed xy images. A maximum-intensity projection (MIP) was then created from the stack for morphological analysis. The criteria to select microglia for analysis included a clearly identifiable soma and processes seen in the x-y plane.

Next, microglial morphological analysis was done using Imaris 9.5 software and the Filament module (Supplementary Fig. 1). The filament created in Imaris is a connected graph-based object consisting of vertices that are connected by edges. Feature extraction by the Filament module yielded microglial features and parameters defined as the following:

Microglial process: Same a filament dendrite in module. Microglial processes form the main structure of the filament object. Processes extend from the microglial cell body and can undergo branching. A process graph is a sequence of vertices connected by edges.

Number of branch points: Same a filament branch depth in module. The process graph is a tree-based structure that has a root point. Branching depth is defined as the number of branches or bifurcations in the shortest path from the beginning point to a given point in the process graph.

Process length: Same a filament dendrite length in module, in reference to the sum of all process lengths within the entire microglial cell.

Microglial surveillance area: Same a filament dendrite area in module, in reference to the sum of all process areas within the entire microglial cell.

Microglial surveillance volume: Same as filament dendrite volume. In volumetric imaging, it is the sum of the volumes of all processes within the microglial cell.

Process end-point speed: Same as filament track speed. The speed is calculated using the "Track over time" function and given by the absolute track length change, whether extension or retraction, divided by the corresponding elapsed time.

NE signals analysis

To analyze NE signals data, we binned the raw data into 1 Hz and subtracted the background autofluorescence. $\Delta F/F_0$ were calculated by using the fluorescence signal itself. Baseline fluorescence was defined as the mean value of the lowest fluorescence signal for 60 consecutive seconds in each recorded fluorescence signal. The z-score transformed $\Delta F/F_0$ was used for analysis. In order to accurately quantify the changes of NE signals in different brain states, wake and NREM states with a duration of more

than 1 min were selected, in which the mean value of 30 seconds fluorescence signal at the end was selected as the NE signal in this state, which was further processed and analyzed combined with video interpretation. Since the duration of REM state is relatively short and it enters a low level at the end of REM, the mean value of fluorescence signal in the 30s before the transition from REM state to wake state is used to represent NE signal in REM state.

Statistical analyses.

Significance levels indicated are as follows: $^{*}P < 0.05$, $^{**}P < 0.01$, $^{***}P < 0.001$. All data are presented as mean ± SEM. All statistical tests used were two-tailed. The overall difference was first evaluated using the ANOVA test. Statistical analyses utilized a paired or unpaired *t*-test design with a two tailed test of significance for changes within a cell across different conditions. All statistical testing was performed using GraphPad Prism 6.0 (GraphPad Software). No statistical methods were used to predetermine sample sizes, but our sample sizes were similar to those reported in previous publications (Davalos et al., 2005b; Nimmerjahn *et al.*, 2005).

References

Bellesi, M., Pfister-Genskow, M., Maret, S., Keles, S., Tononi, G., and Cirelli, C. (2013). Effects of sleep and wake on oligodendrocytes and their precursors. J Neurosci *33*, 14288-14300. 10.1523/JNEUROSCI.5102-12.2013.

Bellesi, M., Tononi, G., Cirelli, C., and Serra, P.A. (2016). Region-specific dissociation between cortical noradrenaline levels and the sleep/wake cycle. Sleep *39*, 143-154. 10.5665/sleep.5336.

Bellesi, M., Vivo, L.D., Chini, M., Gilli, F., Tononi, G., and Cirelli, C. (2017). Sleep loss promotes astrocytic phagocytosis and microglial activation in mouse cerebral cortex. Journal of Neuroscience *37*, 5263-5273. 10.1523/JNEUROSCI.3981-16.2017.

Berridge, C.W., Schmeichel, B.E., and Espana, R.A. (2012). Noradrenergic modulation of wakefulness/arousal. Sleep Med Rev *16*, 187-197. 10.1016/j.smrv.2011.12.003.

Besedovsky, L., Lange, T., and Haack, M. (2019). The sleep-immune crosstalk in health and disease. Physiological Reviews *99*, 1325-1380. 10.1152/physrev.00010.2018.

Chen, X.J., Liu, Y.H., Xu, N.L., and Sun, Y.G. (2021). Multiplexed Representation of Itch and Mechanical and Thermal Sensation in the Primary Somatosensory Cortex. The Journal of neuroscience : the official journal of the Society for Neuroscience *41*, 10330-10340. 10.1523/JNEUROSCI.1445-21.2021.

Corsi, G., Picard, K., di Castro, M.A., Garofalo, S., Tucci, F., Chece, G., Del Percio, C., Golia, M.T., Raspa, M., Scavizzi, F., et al. (2021). Microglia modulates hippocampal synaptic transmission and sleep duration along the light/dark cycle. Glia. 10.1002/glia.24090.

Davalos, D., Grutzendler, J., Yang, G., Kim, J.V., Zuo, Y., Jung, S., Littman, D.R., Dustin, M.L., and Gan, W.B. (2005a). ATP mediates rapid microglial response to local brain injury in vivo. Nature neuroscience *8*, 752-758. 10.1038/nn1472.

Davalos, D., Grutzendler, J., Yang, G., Kim, J.V., Zuo, Y., Jung, S., Littman, D.R., Dustin, M.L., and Gan, W.B. (2005b). ATP mediates rapid microglial response to local brain injury in vivo. Nat Neurosci *8*, 752-758. 10.1038/nn1472.

Eyo, U.B., Mo, M., Yi, M.H., Murugan, M., Liu, J., Yarlagadda, R., Margolis, D.J., Xu, P., and Wu, L.J. (2018). P2Y12R-Dependent Translocation Mechanisms Gate the Changing Microglial Landscape. Cell Rep *23*, 959-966. 10.1016/j.celrep.2018.04.001.

Feng, J., Zhang, C., Lischinsky, J.E., Jing, M., Zhou, J., Wang, H., Zhang, Y., Dong, A., Wu, Z., Wu, H., et al. (2019). A Genetically Encoded Fluorescent Sensor for Rapid and Specific In Vivo Detection of Norepinephrine. Neuron *102*, 745-761 e748. 10.1016/j.neuron.2019.02.037.

Fogel, S.M., and Smith, C.T. (2011). The function of the sleep spindle: a physiological index of intelligence and a mechanism for sleep-dependent memory consolidation. Neuroscience and biobehavioral reviews *35*, 1154-1165. 10.1016/j.neubiorev.2010.12.003.

Frank, M.G. (2019). The Role of Glia in Sleep Regulation and Function. Handbook of experimental pharmacology *253*, 83-96. 10.1007/164_2017_87.

Frank, M.G., and Heller, H.C. (2019). The Function(s) of Sleep. Handbook of experimental pharmacology *253*, 3-34. 10.1007/164_2018_140.

Garcia-Marin, V., Garcia-Lopez, P., and Freire, M. (2007). Cajal's contributions to glia research. Trends in neurosciences *30*, 479-487. 10.1016/j.tins.2007.06.008.

Gonzalez, M.M., Debilly, G., and Valatx, J.L. (1998). Noradrenaline neurotoxin DSP-4 effects on

sleep and brain temperature in the rat. Neuroscience letters *248*, 93-96. 10.1016/s0304-3940(98)00333-4.

Gyoneva, S., and Traynelis, S.F. (2013). Norepinephrine modulates the motility of resting and activated microglia via different adrenergic receptors. Journal of Biological Chemistry *288*, 15291-15302. 10.1074/jbc.M113.458901.

Hall, S., Deurveilher, S., Robertson, G.S., and Semba, K. (2020). Homeostatic state of microglia in a rat model of chronic sleep restriction. Sleep *43*. 10.1093/sleep/zsaa108.

Honda, S., Sasaki, Y., Ohsawa, K., Imai, Y., Nakamura, Y., Inoue, K., and Kohsaka, S. (2001). Extracellular ATP or ADP induce chemotaxis of cultured microglia through Gi/o-coupled P2Y receptors. Journal of Neuroscience *21*, 1975-1982. 10.1523/jneurosci.21-06-01975.2001.

Huisman, Y., Uphoff, K., Berger, M., Dobrindt, U., Schelhaas, M., Zobel, T., Bussmann, J., van Impel, A., and Schulte-Merker, S. (2022). Meningeal lymphatic endothelial cells fulfill scavenger endothelial cell function and cooperate with microglia in waste removal from the brain. Glia *70*, 35-49. 10.1002/glia.24081.

Kierdorf, K., and Prinz, M. (2017). Microglia in steady state. The Journal of clinical investigation *127*, 3201-3209. 10.1172/JCI90602.

Kjaerby, C., Andersen, M., Hauglund, N., Untiet, V., Dall, C., Sigurdsson, B., Ding, F., Feng, J., Li, Y., Weikop, P., et al. (2022). Memory-enhancing properties of sleep depend on the oscillatory amplitude of norepinephrine. Nat Neurosci *25*, 1059-1070. 10.1038/s41593-022-01102-9.

Krueger, J.M., Majde, J.A., and Rector, D.M. (2011). Cytokines in immune function and sleep regulation. Handbook of Clinical Neurology.

Liu, H., Wang, X., Chen, L., Chen, L., Tsirka, S.E., Ge, S., and Xiong, Q. (2021). Microglia modulate stable wakefulness via the thalamic reticular nucleus in mice. Nat Commun *12*, 4646. 10.1038/s41467-021-24915-x.

Liu, Y.U., Ying, Y., Li, Y., Eyo, U.B., Chen, T., Zheng, J., Umpierre, A.D., Zhu, J., Bosco, D.B., Dong, H., and Wu, L.J. (2019). Neuronal network activity controls microglial process surveillance in awake mice via norepinephrine signaling. Nat Neurosci *22*, 1771-1781. 10.1038/s41593-019-0511-3.

Marquez-Ropero, M., Benito, E., Plaza-Zabala, A., and Sierra, A. (2020). Microglial Corpse Clearance: Lessons From Macrophages. Frontiers in immunology *11*, 506. 10.3389/fimmu.2020.00506.

Mori, K., Ozaki, E., Zhang, B., Yang, L., Yokoyama, A., Takeda, I., Maeda, N., Sakanaka, M., and Tanaka, J. (2002). Effects of norepinephrine on rat cultured microglial cells that express α1, α2, β1 and β2 adrenergic receptors. Neuropharmacology *43*, 1026-1034. 10.1016/S0028-3908(02)00211-3.

Nimmerjahn, A., Kirchhoff, F., and Helmchen, F. (2005). Resting microglial cells are highly dynamic surveillants of brain parenchyma in vivo. Science *308*, 1314-1318. 10.1126/science.1110647.

Obenhaus, H.A., Zong, W., Jacobsen, R.I., Rose, T., Donato, F., Chen, L., Cheng, H., Bonhoeffer, T., Moser, M.B., and Moser, E.I. (2022). Functional network topography of the medial entorhinal cortex. Proc Natl Acad Sci U S A *119*. 10.1073/pnas.2121655119.

Pandi-Perumal, S.R., Cardinali, D.P., and Chrousos, G.P. (2007). Neuroimmunology of Sleep 10.1007/978-0-387-69146-6

Rasch, B., and Born, J. (2013). About sleep's role in memory. Physiol Rev *93*, 681-766. 10.1152/physrev.00032.2012.

Stowell, R.D., Sipe, G.O., Dawes, R.P., Batchelor, H.N., Lordy, K.A., Whitelaw, B.S., Stoessel, M.B., Bidlack, J.M., Brown, E., Sur, M., and Majewska, A.K. (2019). Noradrenergic signaling in the wakeful state inhibits microglial surveillance and synaptic plasticity in the mouse visual cortex. Nat Neurosci *22*, 1782-1792. 10.1038/s41593-019-0514-0.

Sugama, S., Takenouchi, T., Hashimoto, M., Ohata, H., Takenaka, Y., and Kakinuma, Y. (2019). Stress-induced microglial activation occurs through β-adrenergic receptor: Noradrenaline as a key neurotransmitter in microglial activation. Journal of Neuroinflammation *16*, 266. 10.1186/s12974-019-1632-z.

Tuan, L.H., and Lee, L.J. (2019). Microglia-mediated synaptic pruning is impaired in sleep-deprived adolescent mice. Neurobiology of Disease *130*, 104517. 10.1016/j.nbd.2019.104517.

Wang, C., Yue, H., Hu, Z., Shen, Y., Ma, J., Li, J., Wang, X.D., Wang, L., Sun, B., Shi, P., et al. (2020). Microglia mediate forgetting via complement-dependent synaptic elimination. Science *367*, 688-694. 10.1126/science.aaz2288.

Wolf, S.A., Boddeke, H.W., and Kettenmann, H. (2017). Microglia in Physiology and Disease. Annual review of physiology *79*, 619-643. 10.1146/annurev-physiol-022516-034406.

Xie, L., Kang, H., Xu, Q., Chen, M.J., Liao, Y., Thiyagarajan, M., O'Donnell, J., Christensen, D.J., Nicholson, C., Iliff, J.J., et al. (2013). Sleep drives metabolite clearance from the adult brain. Science *342*, 373-377. 10.1126/science.1241224.

Zhang, C., Zhu, H., Ni, Z., Xin, Q., Zhou, T., Wu, R., Gao, G., Gao, Z., Ma, H., Li, H., et al. (2022). Dynamics of a disinhibitory prefrontal microcircuit in controlling social competition. Neuron *110*, 516-531 e516. 10.1016/j.neuron.2021.10.034.

Zhang, Y., Chen, K., Sloan, S.A., Bennett, M.L., Scholze, A.R., O'Keeffe, S., Phatnani, H.P., Guarnieri, P., Caneda, C., Ruderisch, N., et al. (2014). An RNA-sequencing transcriptome and splicing database of glia, neurons, and vascular cells of the cerebral cortex. Journal of Neuroscience *34*, 11929-11947. 10.1523/JNEUROSCI.1860-14.2014.

Zong, W., Wu, R., Chen, S., Wu, J., Wang, H., Zhao, Z., Chen, G., Tu, R., Wu, D., Hu, Y., et al. (2021). Miniature two-photon microscopy for enlarged field-of-view, multi-plane and long-term brain imaging. Nat Methods *18*, 46-49. 10.1038/s41592-020-01024-z.

Zong, W., Wu, R., Li, M., Hu, Y., Li, Y., Li, J., Rong, H., Wu, H., Xu, Y., Lu, Y., et al. (2017). Fast high-resolution miniature two-photon microscopy for brain imaging in freely behaving mice. Nat Methods *14*, 713-719. 10.1038/nmeth.4305.

Figures

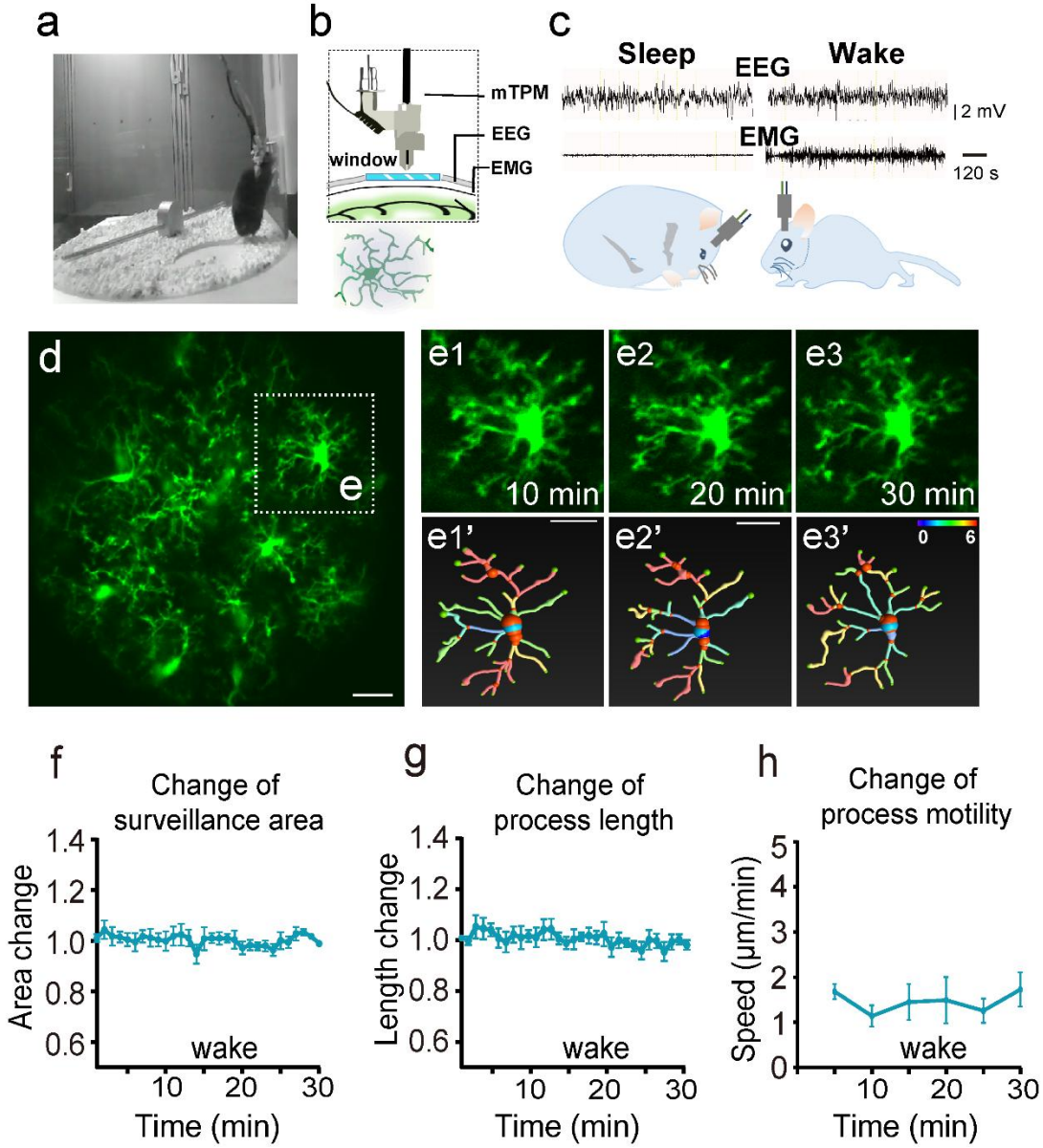

Fig. 1. Imaging microglial surveillance in the somatosensory cortex in freely moving mice.

(a-c) Experimental setup. The animal was head-mounted with a miniature two-photon microscope (mTPM) and EEG/EMG electrodes and behaved freely in a cylindrical chamber (a). Microglia expressing GFP in the somatosensory cortex were imaged through a cranial window using the mTPM (b) and the sleep/wake state of the animal was simultaneously monitored using an EEG/EMG recording system (b-c).

(d-e) Microglial morphological dynamics when the animal was awake. A representative image with a FOV of 220 × 220 μm^2. **(e1-e3)** Expanded views of selected microglia in box from (d) at 10 min (e1), 20 min (e2) and 30 min (e3) of continuous recording. **(e1'-e3')** Microglial process graphs digitally reconstruction for E1-E3 using Imaris software. In Figure e1′-e3′, the branch points of processes are represented in red and the number of different branches of the whole cell is represented as gradient colors.

(f-h) Quantitative analysis of changes in microglia surveillance area (f), process length (g), and process motility, indexed by the speed of the extension and retraction at end points of the processes (h). Note that the gross morphology of microglia remained largely unchanged over a 30-min time frame in the wake state, despite significant motility at the ends of the processes. Scale bars, 25μm.

n = 12 cells from 3 mice. Scale bars, 30μm. See supplementary Fig. 1-3 for more details.

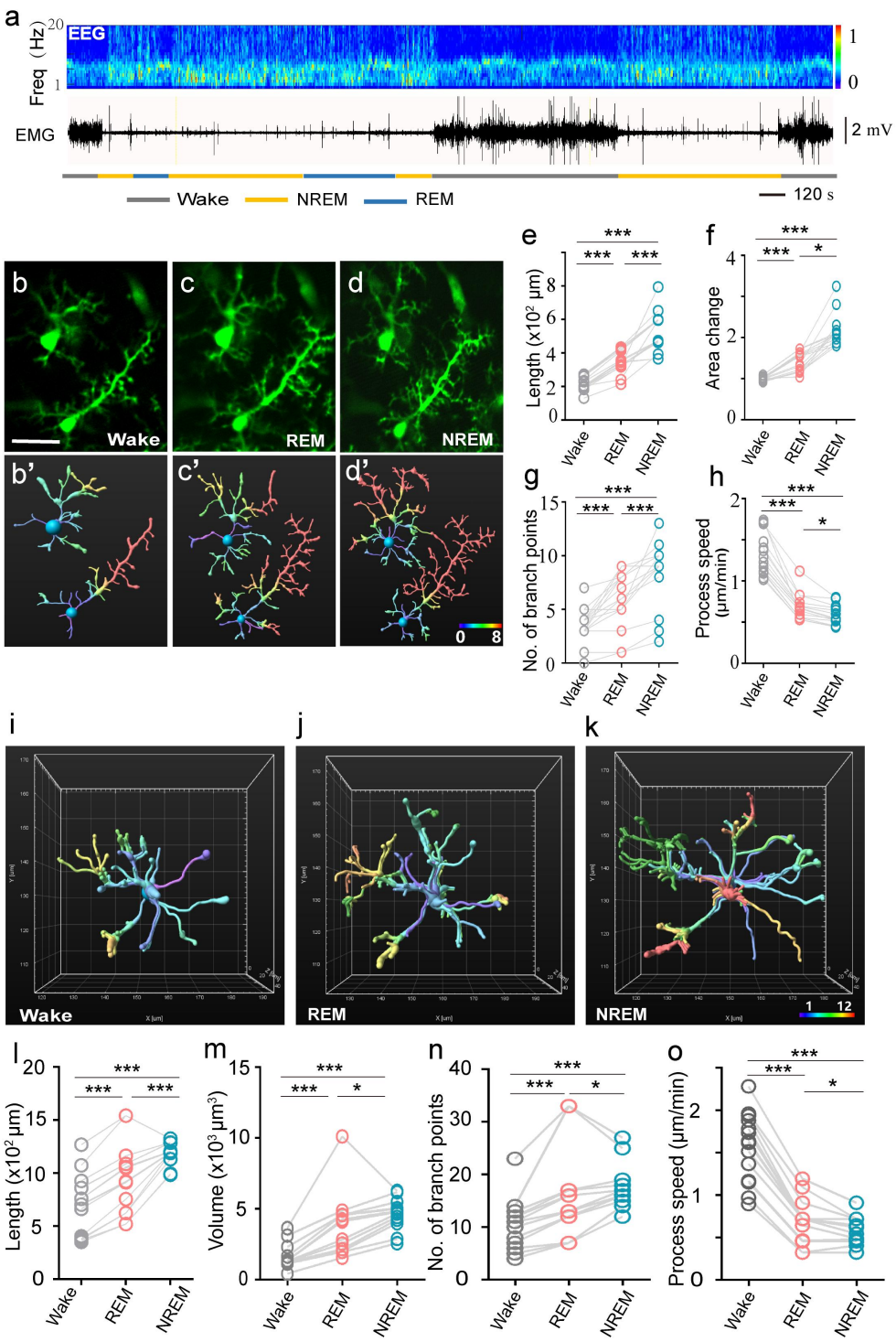

Fig. 2. Microglial surveillance is state-dependent in the sleep-wake cycle.

(a) Representative EEG/EMG recordings showing the sleep-wake stage switch. Top, EEG power spectrogram (1-20 Hz). Middle, EMG trace. Bottom, brain states classified as wake (color code: gray), REM (blue), and NREM (orange).

(b-d) Representative microglial morphological changes during the sleep-wake cycle. **(b′-d′)** Microglial morphology reconstructed from b-d using Imaris software.

(e-h) Microglial morphological parameters, length (e), area change (f), number of branch points (g), and process end point speed (h), all exhibited brain state-dependent dynamic change.

n = 15 cells from 6 mice for each group; *P < 0.05, ***P < 0.001, paired *t*-test (two-tailed).

(i-o) 3D multi-plane imaging and reconstruction of microglial morphology. A 3D ETL lens was used to acquire multi-plane imaging (220*220*40 μm^3) at Z-intervals of 2μm, at a rate of 7.5 stacks/5min.

(i-k) 3D reconstructed microglial morphology in wake (i), REM (j), and NREM (k) states, with corresponding time stamps shown at the bottom.

(l-o) Quantitative analysis of microglial length (l), volume change (m), number of branch points (n), and process motility (o) based on multi-plane microglial imaging. Data from 3D imaging corroborated state-dependent changes of microglial morphology in the sleep-wake cycle. Scale bars, 30μm.

One-way ANOVA test, n = 15 cells from 6 mice for each group; *P < 0.05, ***P < 0.001, paired *t*-test (two-tailed)

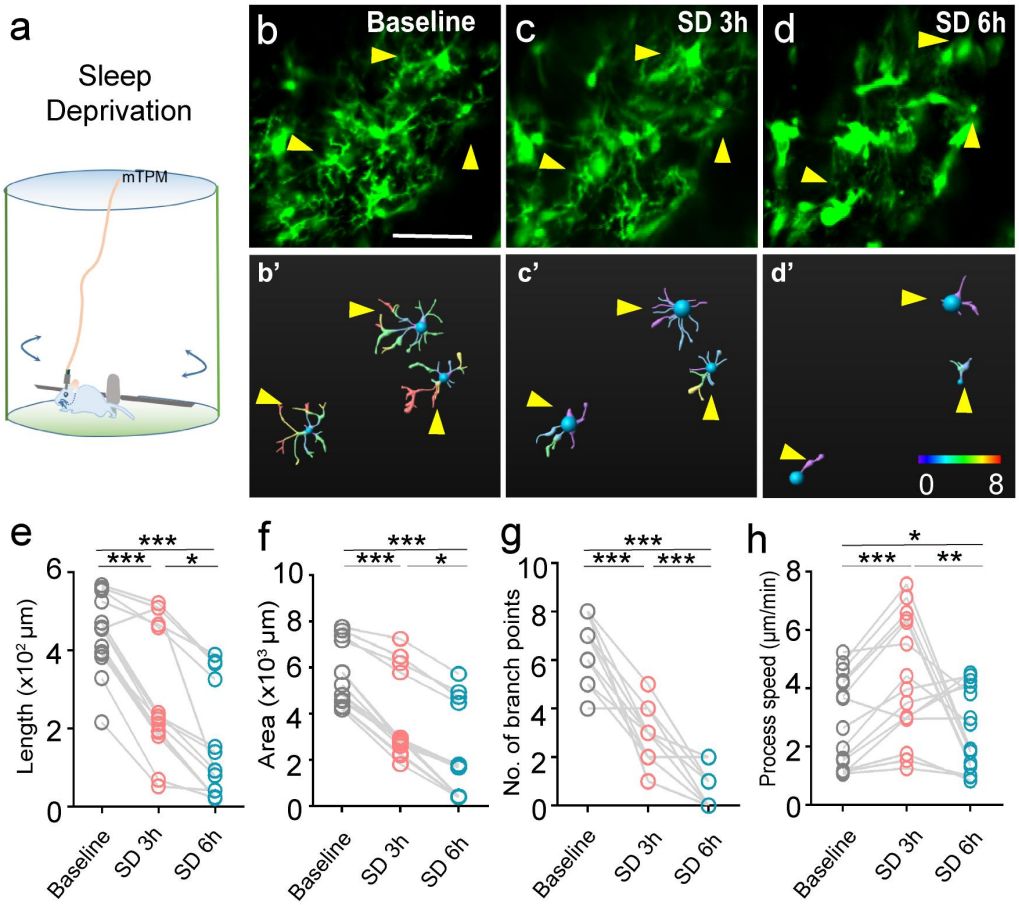

Fig.3. Changes of microglial surveillance in the state of sleep deprivation.

(a) Experimental setup for sleep deprivation. Sleep deprivation in mice was achieved by forcing them to exercise and interrupting their sleep with the rotation of a 46-cm rod (18 turns/ min) in the chamber (diameter 50 cm).

(b-d) Microglial processes contracted after sleep deprivation (SD), baseline (b), SD 3h (c), and SD 6h (d). (b′-d′) Morphological changes of microglia reconstructed using Imaris software. b'-d' correspond to b-d, respectively.

(e-h) Statistics for length (e), area (f), number of branch points (g), and process motility (h). Scale bar, 30 μm.

One-way ANOVA test, n = 15 cells from 6 mice for each group; *P < 0.05, **P < 0.01, ***P < 0.001, paired t-test (two-tailed)

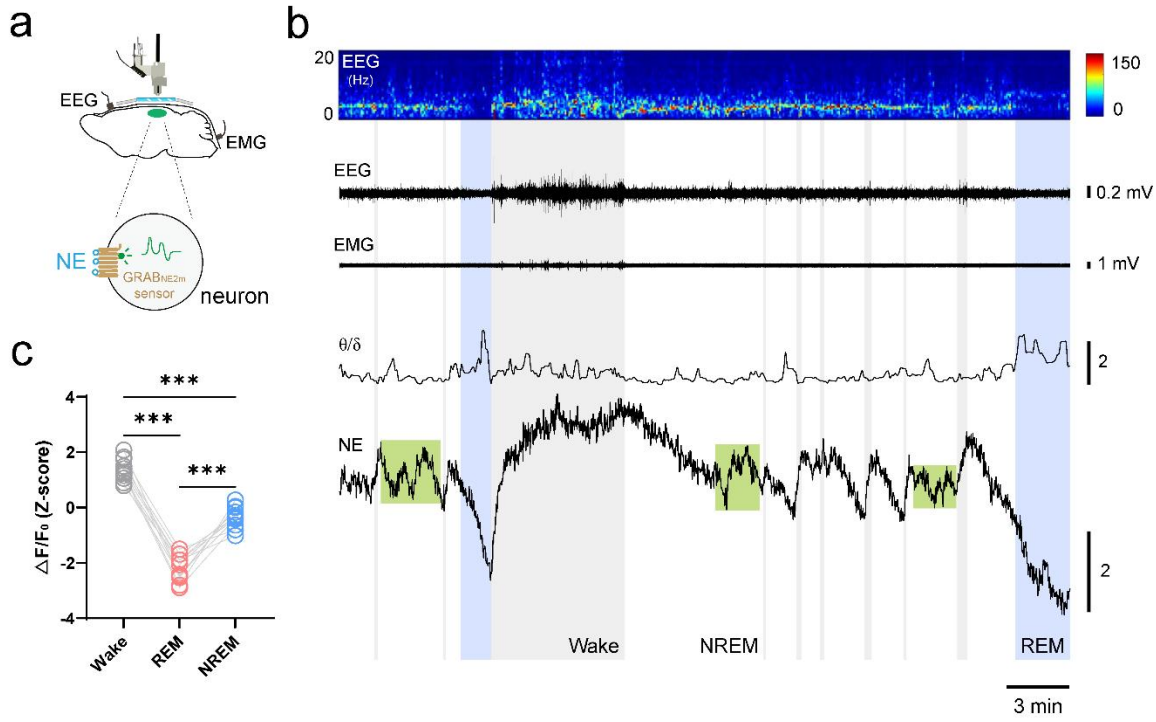

Fig. 4. NE dynamics in mouse somatosensory cortex during the sleep-wake cycle.

(a) Schematic diagram depicting mTPM recording of extracellular NE indicated by the $GRAB_{NE2m}$ sensor expressed in neurons.

(b) Representative traces of simultaneous recordings in the somatosensory cortex during the sleep-wake cycle in freely behaving mice. EEG and its power spectrogram (0-20 Hz); EMG; ratio between EEG theta power (θ) and delta power (δ) (theta frequencies, 6-10 Hz; delta frequencies, 0.5-4 Hz; power, μV^2); NE signals reflected by the z-score of the $GRAB_{NE2m}$ fluorescence. The brain states are color-coded (wake, gray; NREM, white; REM, blue; NE oscillatory during NREM sleep, green).

(c) Mean extracellular NE levels in different brain states. Data from the same recording are connected by lines. ***$P < 0.001$, one-way ANOVA test ($n = 11$ from 3 mice), mean ± SEM.

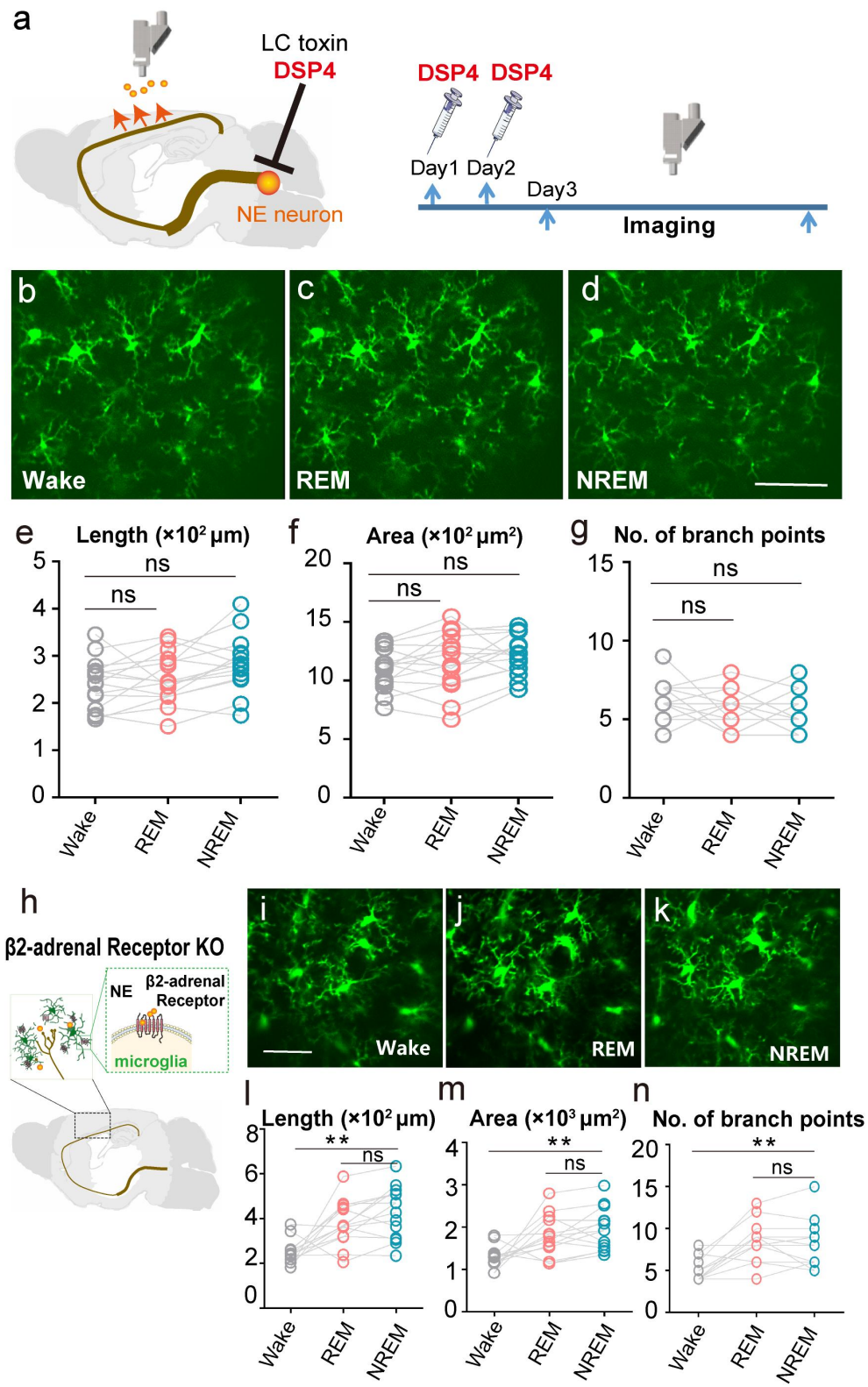

Fig. 5. Microglial surveillance during natural sleep is controlled by LC-NE signal.

(a) Experimental setup: LC-selective neurotoxin DSP4 was used to destroy LC-NE neuronal axons.

(b-g) Lack of sleep/wake state-dependent microglial surveillance in LC- axon ablated animals. b-d: Representative mTPM images of microglia at different states. e-g: Statistics for microglial length (e), surveillance area (f), and number of branch points (g) in LC-axon ablated mice. n = 17 cells from 6 mice for each group; ns, not significant, paired t-test (two-tailed).

(h) Schematic diagram for β_2ARs on the plasma membrane of microglia in the cerebral cortex responding to NE released from axonal terminals projected from LC.

(i-k) State-dependent microglial surveillance during sleep-wake cycle in β_2AR knockout mice. Representative microglial images (i-k) and statistics for microglial process length (l), surveillance area (m), and number of branch points (n) at different states in (CX3CR1-GFP+/-; Adrb2-/-) mice. Scale bar, 30μm.

One-way ANOVA test, n = 15 cells from 6 mice for each group; ns, not significant, $^{**}P < 0.01$, paired t-test (two-tailed).

Supplementary information

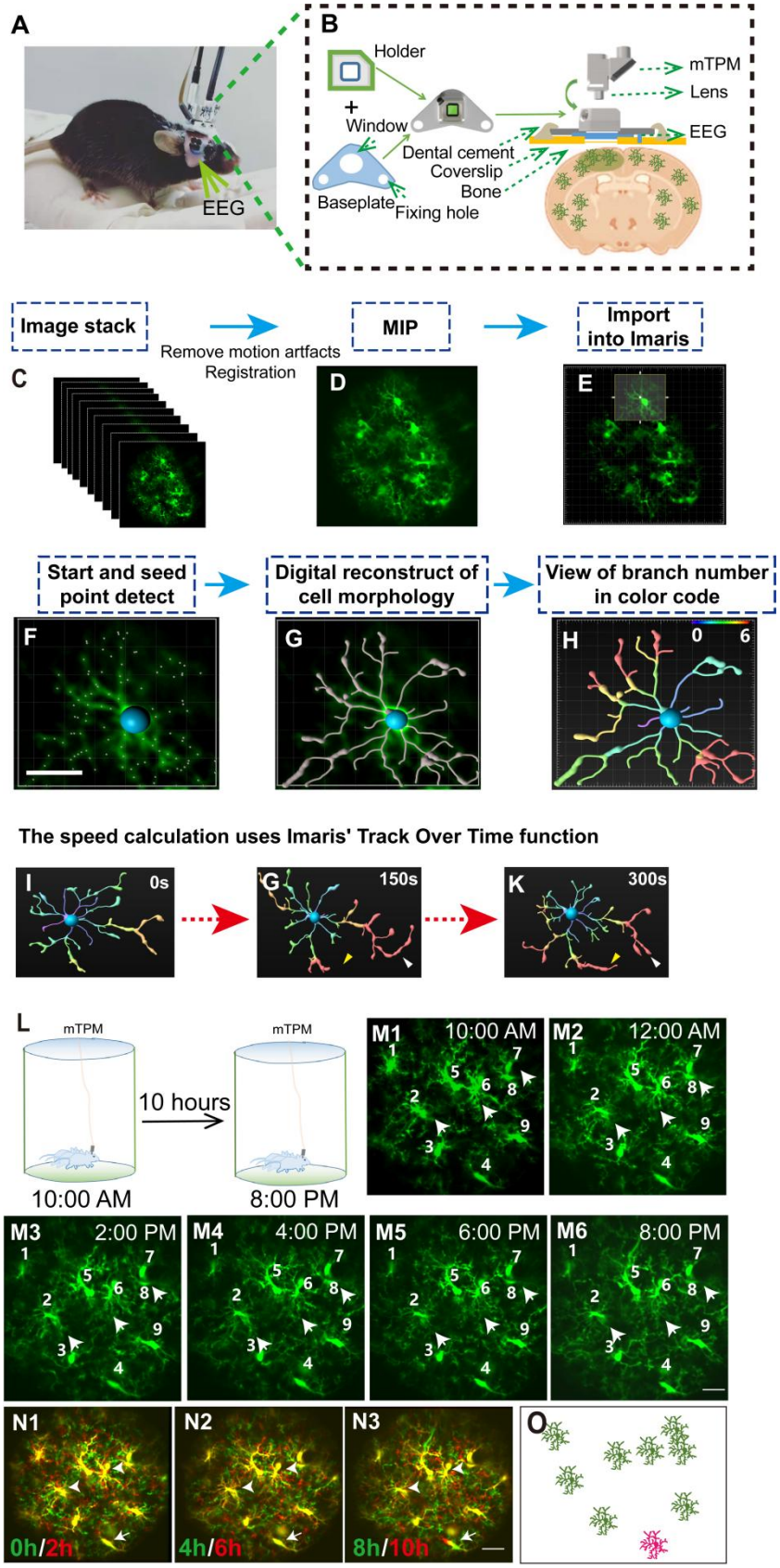

Figure S1. Microglia dynamics imaging and analysis in freely behaving mice. Related to Figure 1.

(A) Head-mounting of the mTPM. Picture of a free moving mouse with a head-mounted mTPM and EEG/EMG recording electrodes.

(B) An illustration showing that the mTPM headpiece was mounted onto an assembly consisting of a baseplate plus a holder glued onto a glass coverslip over a cranial window with dental cement. Initially, the headpiece was screw-fastened to its holder, and their placement on the baseplate was fine-adjusted using a triaxial motorized stage when the animal was immobilized on an imaging stage. The holder was then fixed to the baseplate with dental cement once a proper FOV was located. The animal could then be released and left to move freely in a mouse cage. After an imaging session, dismounting of the headpiece was made easy by unscrewing and unplugging it from the holder.

(C-K) Pipeline for microglial surveillance analysis.

(C-D) An image stack (5-min, 1500 frames) pre-processed using ImageJ software to correct for motion artifacts and to align them using the StackReg plugin. In the case of multi-plane imaging, consecutive z-stacks were first each compressed to single xy projections. A maximum-intensity projection (MIP) was created from the final stack for morphological analysis.

(E) Importing the MIP image to Imaris software and setting ROIs (region of interest) to encompass selected cells with clear cell bodies and processes.

(F-H) For a given cell, Autopath's algorithm was used to find the right starting point and seed point. The radius of process was measured by the shortest distance algorithm. Microglial processes were digitally reconstructed from the calculated seed point and process radius. Each branch was color-coded by its branch point number.

(I-K) Process end-point speed was calculated through Imaris' track-over-time function, the average absolute speed is given by track length divided by time of tracking. Yellow and white arrowheads in (G) and (K) show elongating and contracting process ends, respectively. Scale bar, 20 μm.

(L-O) An example illustrating long-term imaging of microglia in freely behaving mice.

(L) Experimental setup. While the animal was roaming freely in the cage, time-lapse mTPM images were obtained continually at 5 FPS, starting from 10:00 AM and ending at 8:00 PM.

(M) mTPM images of microglia at different time points. Note that no signs of photodamage or photobleaching caused by long-enduring *in vivo* mTPM imaging. All images shown correspond to the wake states of the animal. Numerals identify individual microglia.

(N-O) Overlay of images in (M) for 2h time intervals. Arrows mark the translocation of a cell body (cell number 4). Cartoon in (O) shows that only 1 out 9 microglia cells exhibited local motility (pink) with the rest (green) position unchanged over the duration of observations. Scale bar, 30 μm.

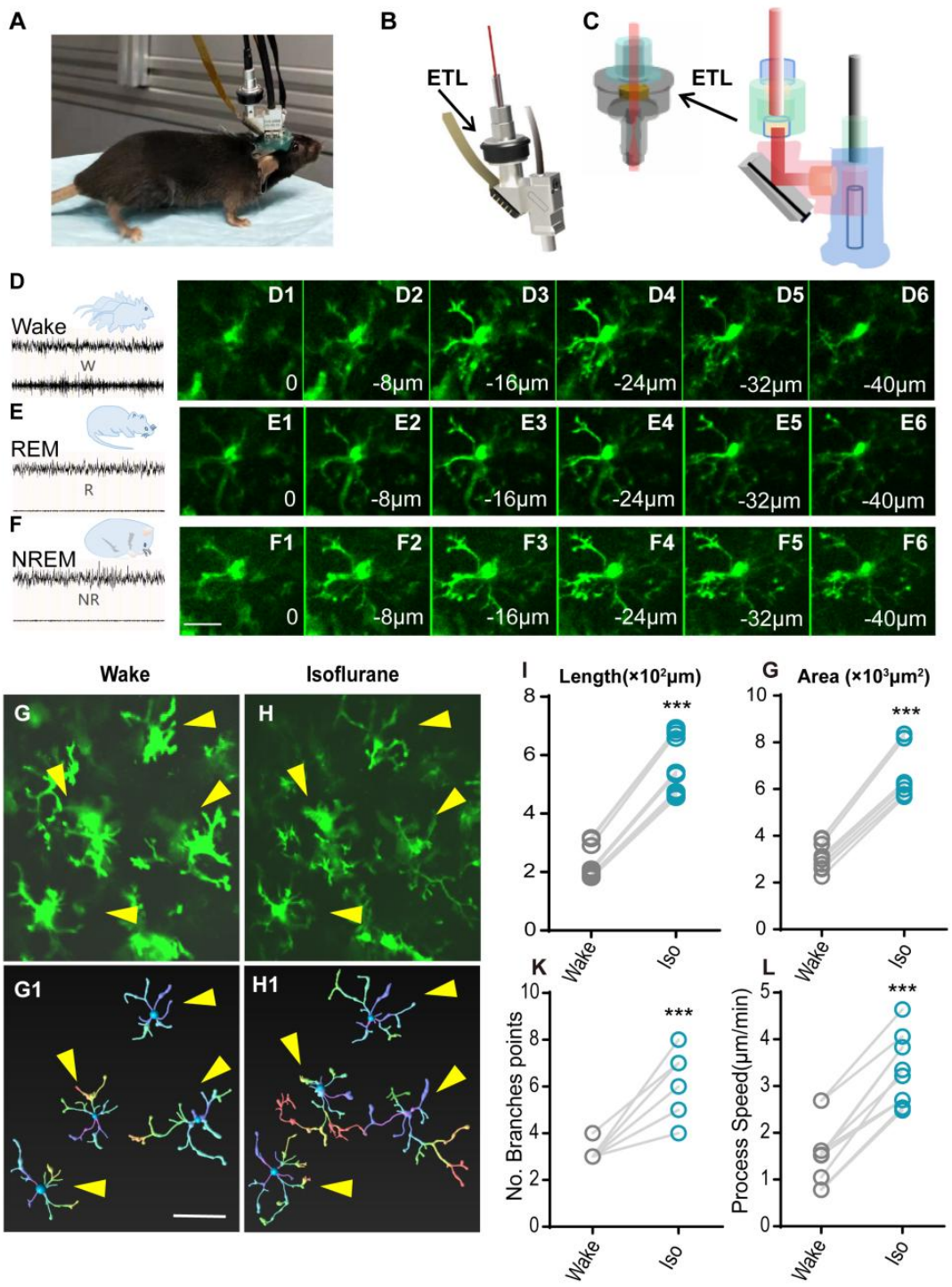

Figure S2. Multiplane imaging of microglial surveillance and changes of microglial surveillance under anesthesia. Related to Figure 2.

(A) Freely behaving mouse wearing an mTPM integrated with an electrical tunable lens (ETL).

(B-C) Schematic of the ETL assembled into the headpiece. The ETL (EL-3-10, Optotune, Dietikon, Switzerland) provided a Z-level change of ~45 μm, allowing for multi-plane imaging.

(D-F) Multi-plane imaging at different wake-sleep states: wake (D), REM (E), and NREM (F). The z-stack could then be used for correction of z-drift artifacts and for 3D analysis of microglial surveillance. Scale bar, 15 μm.

(G-L) Changes of microglial surveillance under anesthesia.

(G-H) Representative micrographs of microglia under wake and anesthetized states. (G1-H1) Digitally reconstructed microglial morphology corresponding to G-H. (I-L) Changes of microglial process length (I), area (G), number of branch points (K), and process end-points speed (L) induced by anesthesia. Scale bar, 30 μm. ***, $P < 0.001$, Wake versus Iso. $n = 12$ cells from 3 mice for each group.

.

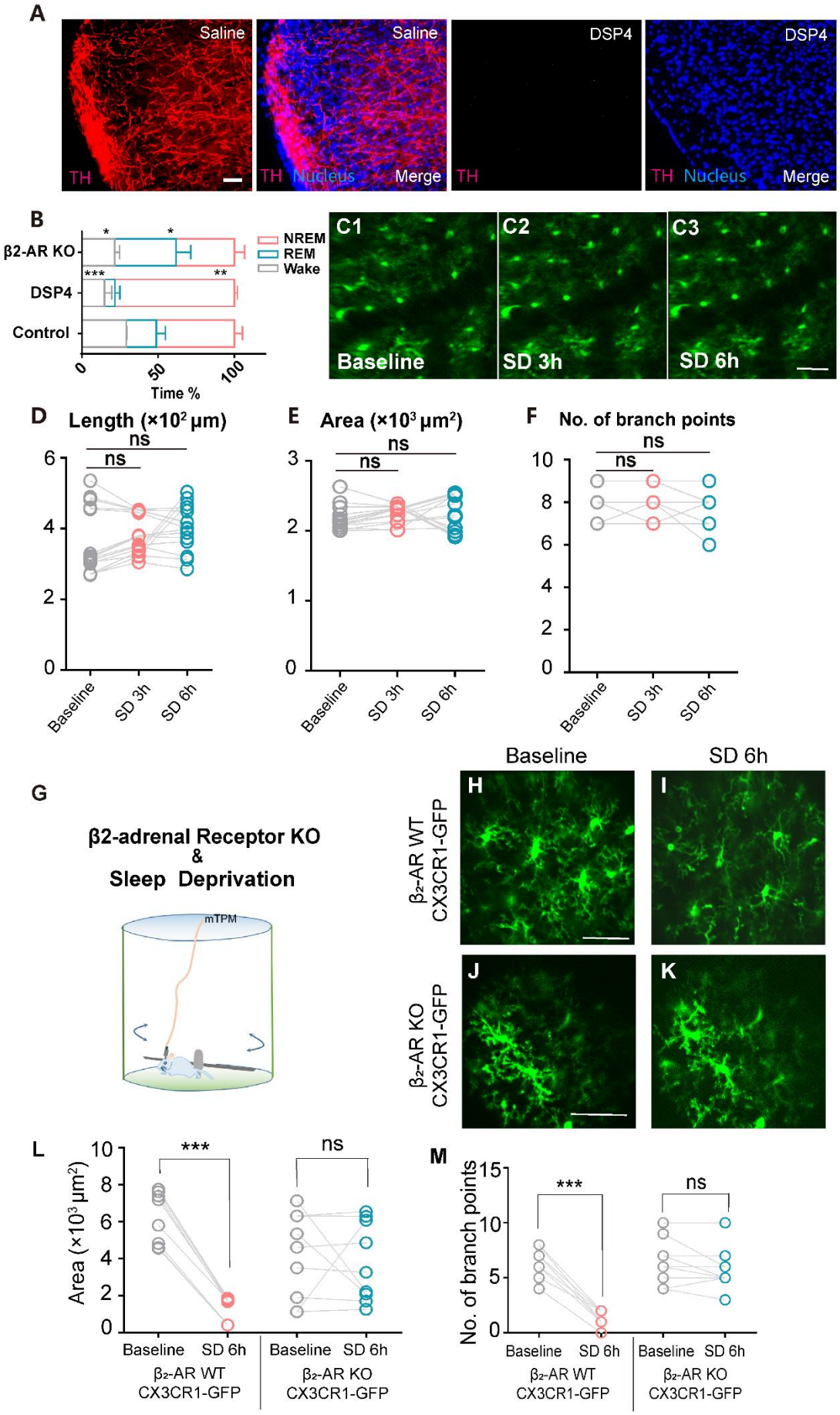
A
Saline
Saline
DSP4
DSP4
TH
TH Nucleus Merge
TH
TH Nucleus Merge
B
β2-AR KO
DSP4
Control
NREM
REM
Wake
Time %
C1
C2
C3
Baseline
SD 3h
SD 6h
D Length (×10² μm)
E Area (×10³ μm²)
F No. of branch points
ns
Baseline
SD 3h
SD 6h
G
β2-adrenal Receptor KO
&
Sleep Deprivation
mTPM
Baseline
SD 6h
β₂-AR WT CX3CR1-GFP
β₂-AR KO CX3CR1-GFP
H
I
J
K
L
Area (×10³ μm²)
***
ns
M
No. of branch points
β₂-AR WT CX3CR1-GFP
β₂-AR KO CX3CR1-GFP

Figure S3. Altered sleep-wake states after DSP4 administration and β_2AR knockout and microglial surveillance during SD is controlled by LC-NE signal. Related to Figure 4.

(A) Tyrosine hydroxylase (TH) expression in somatosensory cortex of mice treated with or without DSP4. Scale bars, 50 μm.

(B) DSP4 treatment and β_2AR knockout both reduced the wake time compared to controls. DSP4 significantly increased NREM time whereas β_2AR KO led to more REM time. $P < 0.05$, $^{**}P < 0.01$, $^{***}P < 0.001$ vs control, $n = 3$ mice for each group, unpaired *t*-test (two-tailed).

(C-F) Lack of microglial surveillance in LC-axon ablated animals. B: Representative mTPM images of microglia during SD. C-E: Statistics for microglial length (C), surveillance area (D) and number of branch points (E) in LC-axon ablated mice.

n =12 cells from 3 mice for each group; ns, not significant, one-way ANOVA with Tukey's multiple comparisons test.

(G-M) Lack of SD-dependent changes in microglial surveillance in the absence of β_2AR signaling.

(G) Experiment setup. (H-I) Representative mTPM micrographs from a (Cx3cr1-GFP+/-; Adrb2+/+) mouse. (J-K) Representative mTPM micrographs from a (Cx3cr1-GFP+/-; Adrb2-/-) mouse. No significant morphological changes were observed in β_2AR KO mouse after SD. (L-M) Quantitative analysis of changes in microglial surveillance area (L) and number of branch points (M) in WT and β_2AR KO mice.

Scale bars, 30 μm.

n = 9 cells from 3 mice for each group; ns, not significant, ***$P < 0.001$.